

Numerical and Computational Methods in Sciences & Engineering An International Journal

http://dx.doi.org/10.18576/ncmse/060101

Effects of Wall Permeability in Unsteady Generalized Couette Flow of Nanofluid with Convective Heating

M. H. Mkwizu^{1,*}, A. X. Matofali¹ and G. K. Karugila¹

¹ Department of Mathematics and Statistics, College of Natural and Applied Sciences, Sokoine University of Agriculture-Tanzania

Received: 1 Oct. 2024, Revised: 20 Dec. 2024, Accepted: 27 Jan. 2025.

Published online: 1 Mar. 2025.

Abstract: This study explores how wall permeability affects unsteady Couette flow in a nanofluid with convective heating. We developed a flow model to analyze how different parameters influence velocity, temperature, and entropy generation, including the role of magnetic fields. The results show that higher nanoparticle concentration and Reynolds number boost velocity when pressure gradient, MHD effects, and nanofluid fraction stay fixed. Interestingly, Alumina-water nanofluid accelerates flow faster than Copper-water nanofluid. Meanwhile, increasing the Eckert number lowers the temperature profile, with copper-water nanofluid heating up more quickly than Alumina-water. Another key finding is that entropy generation grows with the Eckert number but behaves differently along the channel it raises near the lower wall but drops closer to the upper wall as nanoparticle concentration increases. These insights could help optimize nanofluid applications in thermal systems and magnetic-field-controlled flows.

Keywords: Couette flow, nanofluid, wall permeability, Convective Heating.

1 Introduction

Fluid flows play a crucial role in both natural phenomena and engineered systems, shaping processes ranging from stellar evolution and atmospheric dynamics to sound propagation, transportation, and energy conversion. Understanding the mechanics and thermodynamics of fluid motion is vital for designing aircraft, propulsion systems, and power generation technologies.

In practical engineering applications, nanofluid flow is frequently encountered within mechanical systems. Among the fundamental flow configurations observed in such systems is Couette flow, which represents shear-driven motion between two parallel plates, where one plate moves tangentially relative to the other while the other remains stationary. This flow phenomenon is commonly present in fluid machinery involving moving components and plays a significant role in hydrodynamic lubrication processes [1,2]. Couette flow can manifest in various forms steady or unsteady, compressible or incompressible, viscous or inviscid, and rotational or irrotational reflecting both the intrinsic properties of the fluid and the characteristics of its motion [1,2].

The term nanofluid, as introduced by [3], refers to a stable suspension of nanoscale particles (typically smaller than 100 nm) dispersed within a base fluid. These engineered fluids exhibit enhanced thermophysical properties even at relatively low nanoparticle concentrations, making them highly effective for heat transfer and fluid flow applications. Nanoparticles can be synthesized from a wide range of materials, including metals (Cu, Ag, Au, Al, and Fe), oxide ceramics, nitride ceramics, carbide ceramics (SiC, TiC), semiconductors, carbon nanotubes, and composite materials such as alloyed nanoparticles or nanoparticle—polymer core—shell composites [4].

Convective heat transfer using nanofluids has attracted substantial research interest due to their remarkable potential for enhancing thermal performance in engineering systems. Nanofluids have been employed across diverse sectors, including transportation, energy production, and advanced electronic systems such as microprocessors and micro-electromechanical devices. They are also widely utilized in engine cooling systems, solar energy collectors, nuclear reactor cooling, metallurgy, polymer extrusion, and thermal therapies for cancer treatment. Additionally, nanofluids are applied in chemical processing, ventilation, and air-conditioning systems, as well as in the cooling of automobile engines, welding equipment, and high-heat-flux devices such as high-power microwave tubes and laser diode arrays [15].

Several numerical and experimental studies have explored the behavior of nanofluids in Couette flow and related thermal systems. For instance, [6] conducted a numerical investigation on entropy generation in unsteady magnetohydrodynamic (MHD) generalized Couette flow with convective cooling. The study demonstrated that increasing nanoparticle concentration and Reynolds number led to a higher fluid velocity, while the pressure gradient, magnetic field strength, and nanofluid fraction were kept constant. The Alumina–water nanofluid showed a more pronounced velocity enhancement



than the Copper-water nanofluid, whereas an increase in the Eckert number reduced the temperature profile, with copper-water nanofluid exhibiting higher temperatures than Alumina-water nanofluid. Entropy generation was found to increase with the Eckert number, being higher near the lower plate and decreasing toward the upper plate as nanoparticle concentration increased.

Moreover, [7] reported that, compared with other nanostructured materials dispersed in base fluids, carbon nanotubes demonstrate anomalously high heat transfer enhancement, exceeding theoretical predictions. The heat transfer performance also exhibits a nonlinear relationship with nanotube loading, thereby broadening the potential applications of nanotube-based nanofluids. These findings collectively highlight the critical role of nanoparticle type, concentration, and flow parameters in governing heat transfer and entropy generation in nanofluid-based Couette flow systems.

The study by [8] investigated the effects of Navier slip and wall permeability on entropy generation in unsteady generalized Couette flow of nanofluids with convective cooling. The results indicated that an increase in nanoparticle volume fraction and Reynolds number led to a reduction in the velocity profile, whereas the nanofluid velocity increased with an increase in the pressure gradient. Furthermore, the temperature profile was observed to rise with increasing nanoparticle volume fraction, slip parameter, and Eckert number, but decreased with an increase in the Biot number. The entropy generation rate was found to increase with nanoparticle volume fraction and slip parameter; however, it decreased near the lower wall and increased near the upper wall as the Biot number increased.

In a related study, [9] developed a magnetohydrodynamic (MHD) model of nanofluids in a permeable channel with porosity. The flow of electrically conducting nanofluids was analyzed under the influence of a transverse magnetic field, and analytical solutions were obtained using the perturbation method. The results demonstrated that nanofluid velocity increased with the volume fraction, radiation, and permeability parameter in the case of suction, whereas an opposite behavior was observed under injection. Additionally, the velocity of Ag nanofluids decreased with an increase in the magnetic parameter, while injection led to an opposite trend. The study further revealed that different types of nanoparticles exert distinct effects on both velocity and temperature profiles, depending on the suction or injection conditions.

Similarly, [10] developed a model for entropy analysis in nanofluid flow over a stretching sheet in the presence of heat generation/absorption and partial slip. The results showed that entropy generation due to thermal diffusion is the dominant contributor to total entropy production. In particular, increases in the heat source/sink parameter and the dimensionless slip factor resulted in thicker thermal boundary layers and higher temperature profiles, while the Nusselt number and the entropy generation number decreased.

Furthermore, [11] examined the effects of variable viscosity in unsteady nanofluid flow within a pipe with a permeable wall and convective cooling. The study revealed that nanofluid velocity increased with higher variable viscosity, Eckert number, pressure gradient, and suction, while it decreased with increasing Biot number and injection. The temperature of the nanofluid near the pipe wall increased with higher Eckert number and viscosity parameter but decreased due to convective heat loss to the ambient in accordance with Newton's law of cooling. Additionally, the temperature decreased with both suction and injection. The study also observed that nanoparticle volume fraction at the pipe centerline increased with higher Biot number, viscosity parameter, Eckert number, and thermophoresis, whereas it decreased under Brownian motion effects.

The study by [4] examined the combined effects of buoyancy force and Navier slip on MHD flow of a nanofluid over a convectively heated vertical porous plate. The authors analyzed the influence of a magnetic field on the boundary layer flow of an incompressible electrically conducting water-based nanofluid under Navier slip conditions. Their results indicated that fluid velocity increased while local skin friction decreased with an increase in the slip parameter; conversely, velocity decreased with increasing magnetic field intensity, nanoparticle volume fraction, Eckert number, Grashof number, and suction/injection parameter. Both the temperature profile and thermal boundary layer thickness were enhanced by higher magnetic field intensity, nanoparticle volume fraction, Eckert number, and Newtonian heating, whereas the convective cooling effect on the plate surface was strengthened by increased velocity slip and suction.

In a complementary study, [12] performed a thermodynamic analysis of variable viscosity MHD unsteady generalized Couette flow with permeable walls, employing both the first and second laws of thermodynamics. The study revealed that fluid velocity and temperature increased with time across the channel until steady state was achieved, with velocity profiles attaining steady state faster than temperature profiles. The results further demonstrated that an increase in Reynolds number or viscosity exponent enhanced fluid motion toward the upper moving plate, whereas a higher magnetic field parameter increased fluid motion toward the lower fixed plate. Local entropy generation rate increased with the group parameter but decreased with the viscosity exponent. Furthermore, increasing the magnetic field parameter reduced entropy production at the moving upper plate, while a higher Reynolds number decreased entropy generation at the lower fixed plate. Variations in fluid viscosity and group parameter also influenced the Bejan number, with a decrease in viscosity increasing Bejan number, and an increase in the group parameter reducing it.

The study by [13] investigated natural convection in partially heated rectangular enclosures filled with nanofluids. The analysis considered enclosures of different aspect ratios and nanoparticle volume fractions, revealing that heat transfer was more pronounced at low aspect ratios and higher nanoparticle concentrations. The work of [2] focused on entropy generation in hydromagnetic Couette flow of nanofluids within a rotating channel. The findings showed that nanofluid temperature increased with both solid volume fraction and Eckert number. The rotation parameter was positively correlated with entropy generation, and the moving wall of the channel acted as a strong concentrator of irreversibility due to high velocity and temperature gradients. Additionally, the group parameter had a significant effect on entropy generation rate, with higher values leading to increased entropy production.

2 Mathematical Model

Consider an unsteady laminar flow of viscous, incompressible nanofluids containing a specified type of nanoparticles suspended in a base fluid within a Couette flow channel bounded by permeable walls. It is assumed that the fluid is injected uniformly through the lower plate, while uniform suction occurs at the moving upper plate, as illustrated in Figure 1.

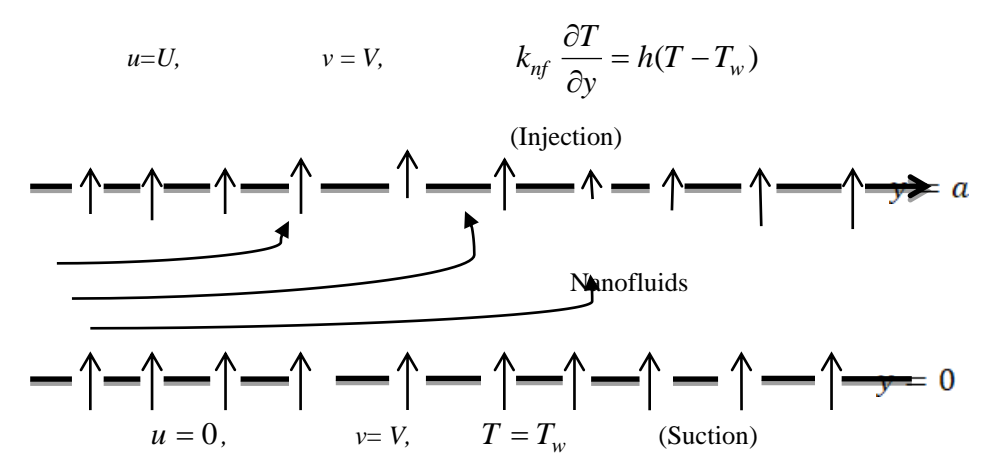


Fig. 1: Schematic diagram of the problem under consideration

Based on the assumptions described above, the governing one-dimensional momentum and energy equations for the nanofluid can be expressed as follows:

$$\frac{\partial u}{\partial \xi} + V \frac{\partial u}{\partial y} = -\frac{1}{\rho_{nf}} \frac{\partial P}{\partial x} + \mu_{nf} \frac{\partial^2 u}{\partial y^2} \tag{1}$$

$$\frac{\partial T}{\partial \bar{t}} + v \frac{\partial T}{\partial y} = \alpha_{\rm nf} \frac{\partial^2 T}{\partial y^2} + \frac{\alpha_{\rm nf} \mu_{\rm nf}}{k_{\rm nf}} \left(\frac{\partial u}{\partial y}\right)^2 \tag{2}$$

where u is the nanofluid velocity in the x-direction, T is the temperature of the nanofluid, P is the nanofluid pressure, t is the time, a is the channel width, T_w is the lower stationary wall temperature, μ_{nf} is the dynamic viscosity of the nanofluid, -

 k_{nf} is the nanofluid thermal conductivity, ρ_{nf} is the density of the nanofluid and α_{nf} is the thermal diffusivity of the nanofluid, which are defined as follows:

$$\mu_{\rm nf} = \frac{\mu_{\rm f}}{(1 - \varphi)^{2.5}},\tag{3}$$

$$\rho_{\rm nf} = (1 - \varphi)\rho_{\rm f} + \varphi \rho_{\rm s},\tag{4}$$

$$\tau = \frac{(\rho c_p)_s}{(\rho c_p)_f} \tag{5}$$

$$\frac{k_{nf}}{k_f} = \frac{(k_s + 2k_f) - 2\phi(k_f - k_s)}{(k_s + 2k_f) + \phi(k_f - k_s)}$$
(6)

$$(\rho c_{p})_{nf} = (1 - \phi)(\rho c_{p})_{f} + \phi(\rho c_{p})_{s}$$

$$(7)$$



where φ represents nanoparticles volume fraction, ρ_f represent density of the base fluid and ρ_s is the density of the nanoparticle, k_f is thermal conductivities of the base fluid and k_s is thermal conductivities of the nanoparticles, the heat capacitance of the base fluid and the nanoparticles are represented by $(\rho c_p)_f$ and $(\rho c_p)_s$ respectively, with appropriate initial and boundary conditions.

$$u(y,0) = 0, \quad T(y,0) = T_w$$
 (8)

$$u(0,t) = 0, T(0,t) = T_w$$
(9)

$$u(a,t) = U, \quad k_{nf} \frac{\partial T}{\partial y}(a,t) = h[(a,t) - T_w)]$$

$$\tag{10}$$

Table 1 presents thermo-physical properties of water, copper and alumina at a given temperature.

Table 1: Thermo-physical Properties Physical properties Fluid phase Alumina Copper (water) Cu Al_2O_3 4179 385 765 997.1 8933 3970 k(W/m K 0.613 401 40

The following are dimensionless quantities:

$$\theta = \frac{T - T_{w}}{T_{w}}, w = \frac{u}{v}, \bar{t} = \frac{tV}{a}, v = \frac{\mu_{f}}{\rho_{f}}, Re = \frac{V_{a}}{v_{f}}, \alpha_{f} = \frac{k_{f}}{(\rho c_{p})_{f}}$$

$$\bar{P} = \frac{\rho_{a}}{\mu_{f}v}, A = \frac{\partial \bar{P}}{\partial X}, X = \frac{x}{a}, \eta = \frac{y}{a}, Pr = \frac{\mu_{f}c_{pf}}{k_{f}}, EC = \frac{v^{2}}{c_{pf}T_{a}},$$

$$m = \frac{(k_{s} + 2k_{f}) + \varphi(k_{f} - k_{s})}{(k_{s} + 2k_{f}) + \varphi(k_{f} - k_{s})}, \tau = \frac{(\rho c_{p})_{s}}{(\rho c_{p})_{f}}$$
(11)

Where Pr denotes the Prandtl number, Ec represents the Eckert number, Re is the Reynolds number, and A denotes the pressure gradient parameter. By substituting Equations (8) – (11) into Equations (1) and (2), the dimensionless governing equations, together with the corresponding initial and boundary conditions, are obtained as follows:

$$\frac{\partial W}{\partial t} = -\frac{A}{Re(1-\varphi+\varphi\rho_s/\rho_f)} + \frac{1}{Re(1-\varphi+\varphi\rho_s/\rho_f)(1-\varphi)^{2.5}} \frac{\partial^2 W}{\partial \eta^2} - \frac{\partial W}{\partial \eta}$$
(12)

$$\frac{\partial \theta}{\partial t} = \frac{1}{mPrRe(1-\varphi+\varphi\tau)} \frac{\partial^2 \theta}{\partial \eta^2} + \frac{Ec}{Re(1-\varphi)^{2.5}(1-\varphi+\varphi\tau)} \left(\frac{\partial W}{\partial \eta}\right)^2 - \frac{\partial \theta}{\partial \eta}$$
(13)

The initial and boundary conditions corresponding to Equations (12) and (13) can be expressed as follows:

$$W(\eta, 0) = \theta(\eta, 0) = 0 \tag{14}$$

$$W(0,t) = 0, \, \theta(0,t) = 0 \tag{15}$$

$$W(1,t) = 1, \frac{\partial \theta}{\partial \eta}(1,t) = -m\beta i\theta(1,t) \tag{16}$$

For numerical solution, the spatial derivatives in Equations (12)- (13) are discretized using second-order accurate central finite difference schemes. This formulation reduces the governing equations to a system of nonlinear ordinary differential equations in the initial value form. The resulting coupled equations are solved iteratively using the Runge-KuttaFehlberg adaptive step-size integration algorithm, implemented computationally through MATLAB programming.

By applying the semi-discretization finite difference method, the nonlinear initial boundary value problem (IBVP) represented by Equations (12)-(16) can be solved numerically. The spatial domain is divided into equal subintervals, and the grid size and corresponding grid points are defined. The first and second spatial derivatives in Equations (12) and (13) are approximated using second-order central finite differences. Consequently, the semi-discrete form of the system

$$\frac{dW}{dt} = \frac{-A}{Re(1 - \varphi + \varphi \rho_s / \rho_f)} + \frac{W_{i+1} - 2W_i + W_{i-1}}{Re(1 - \varphi + \varphi \rho_s / \rho_f)(1 - \varphi)^{2.5} (\Delta \eta)^2} - \frac{W_{i+1} - W_{i-1}}{2\Delta \eta}$$
(17)

$$\frac{d\theta}{dt} = \frac{\theta_{i+1} - 2\theta_i + \theta_{i-1}}{mPrRe(1 - \varphi + \varphi \tau)(\Delta \eta)^2} + \frac{Ec}{Re(1 - \varphi + \varphi \tau)(1 - \varphi)^{2.5}} \left(\frac{W_{i+1} - W_{i-1}}{2\Delta \eta}\right)^2 - \frac{\theta_{i+1} - \theta_{i-1}}{2\Delta \eta}$$
(18)

With initial conditions

becomes:

$$W_i(0) = \theta_i(0) = 0, 1 \le i \le N + 1 \tag{19}$$

And boundary conditions

$$W_1 = 0, \theta = 0, W_{N+1} = 1, \theta_{N+1} = \theta_N (1 - mBi\Delta\eta)$$
 (20)

3 Results and Discussion

To understand the dynamics of the proposed model shown in Figure 1, an in-depth analysis has been carried out with a strong focus on the velocity profiles, temperature profiles, and the effects of varying parameters on these profiles. The behavior and interpretation of the results are thoroughly discussed and supported by detailed explanations and graphical representations in this section.

3.1 Effects of Parameter Variation on Velocity Profiles

The effects of parameter variations on the velocity profiles are illustrated in Figures 2-6. Figure 1 shows that the velocity increases with time for a given set of parameter values until a steady-state profile is reached. It is also observed that the alumina-water nanofluid tends to flow faster than the copper-water nanofluid. This behavior can be attributed to the difference in density between the two nanofluids, as copper nanoparticles have a higher density compared to alumina nanoparticles.

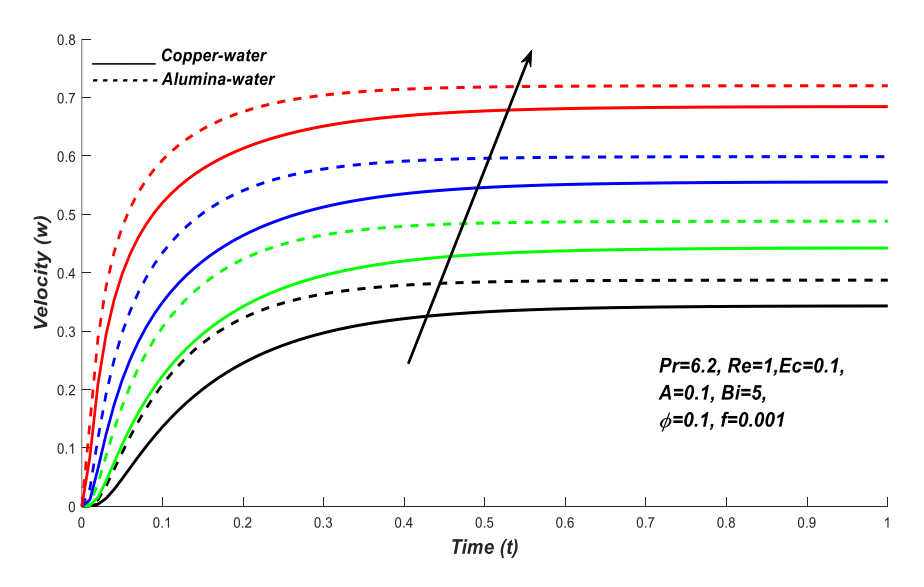


Fig. 2: Nanofluids velocity profiles with increasing time

From Figure 2, it can be observed that as the spatial coordinate increases, the velocity of the nanofluid also increases. The results further indicate that the alumina-water nanofluid exhibits a faster rise in velocity compared to the copper-water nanofluid, which can be attributed to the higher density of copper nanoparticles relative to alumina nanoparticles. In summary, the nanoparticles significantly influence the flow behavior within a small spatial region and over a short time interval.

Figure 3 illustrates that the velocity of copper-water nanofluid particles increases with an increase in spatial position. Similarly, Figure 4 shows that an increase in the pressure gradient parameter (A) leads to a rise in the velocity profile. In other words, the observation indicates that the velocity becomes more significant as the pressure gradient increases.



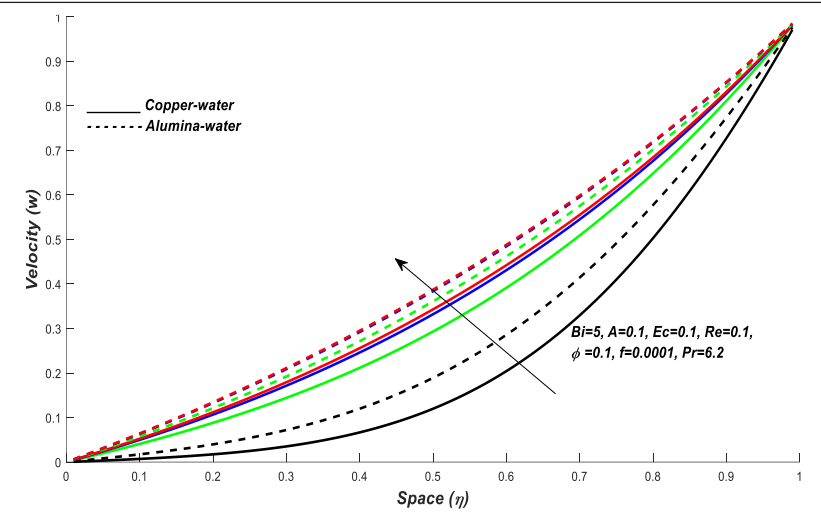


Fig. 3: Nanofluids velocity profiles with increasing space

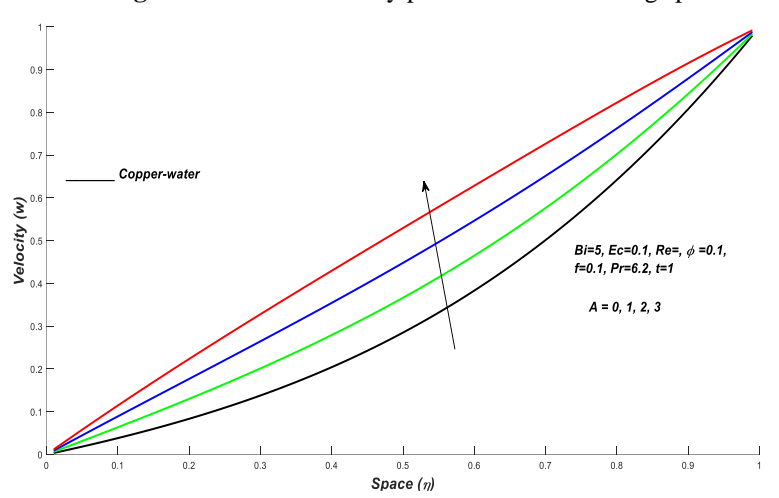


Fig. 4: Nanofluid velocity profiles for different values of pressure gradient parameter (A)

From Figure 5, it is observed that an increase in the nanoparticle volume fraction (Φ) causes a slight decrease in the velocity profile. This behavior may be attributed to factors such as the nanofluid's density, dynamic viscosity, slip conditions, and the effects of suction or injection at the boundary.

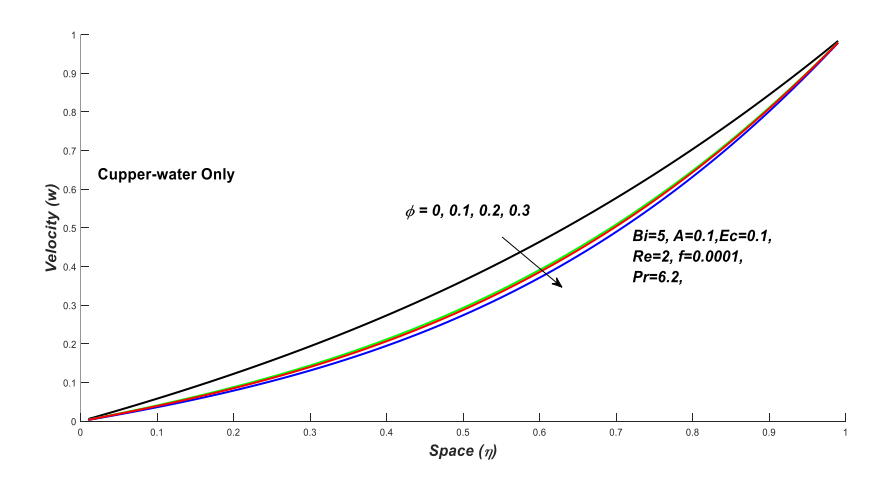


Fig. 5: Nanofluids velocity profile for different values of volume fraction (Φ)

Figure 6 presents the nanofluid velocity profiles for different values of the Reynolds number (Re). It is observed that variations in the Reynolds number have no significant effect on the velocity profile. This behavior may be attributed to the increased viscous forces within the flow system or channel, which counteract the influence of inertial effects.

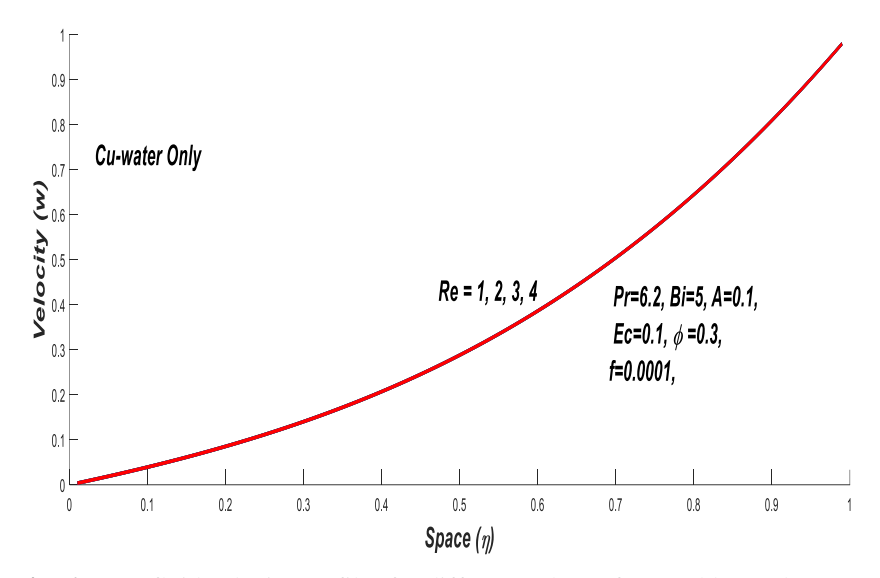


Fig. 6: Nanofluid velocity profiles for different values of Reynolds number (Re)

3.2 Effects of Parameter Variation on Temperature Profiles

Figures 7–11 illustrate the temperature profiles of nanofluids across the channel and the effects of various parameters on the fluid flow system. In general, due to convective heat loss to the surrounding environment, following Newton's law of cooling, the nanofluid temperature near the channel walls decreases. Figure 7 shows that the temperature profile initially increases with time for $0 \le t < 0.2$ and then decreases for $t \ge 0.2$. Additionally, it is observed that the copper-water nanofluid exhibits a faster rise in temperature near the wall compared to the alumina-water nanofluid. This behavior can be attributed to the difference in specific heat capacities, as copper-water nanofluid is a better conductor of heat than alumina-water nanofluid. The figure also indicates that, over time, the alumina-water nanofluid loses temperature more rapidly than the copper-water nanofluid.

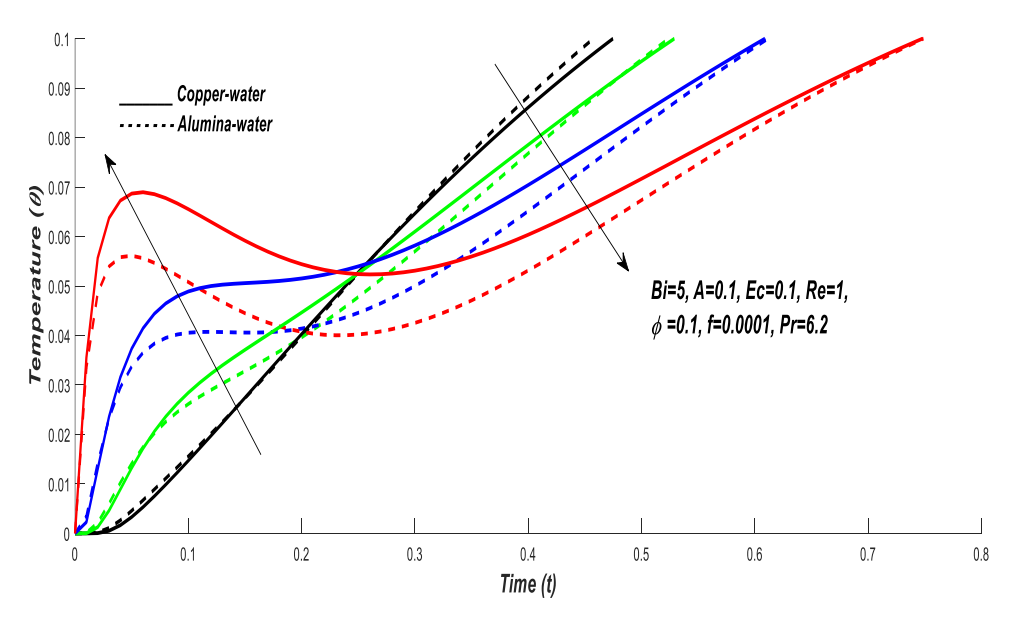


Fig. 7: Temperature profiles of Nanofluids with increasing time

Figure 8 presents the temperature variation profiles for the combined nanofluids, alumina-water and copper-water. The

results indicate that the temperature increases with increasing spatial position. It is observed that the alumina-water nanofluid exhibits a faster rise in temperature for the spatial range $0 \le \eta < 0.65$, which may be attributed to differences in specific heat capacity and density. However, beyond $\eta = 0.65$, the copper-water nanofluid shows a more rapid increase in temperature compared to the alumina-water nanofluid.

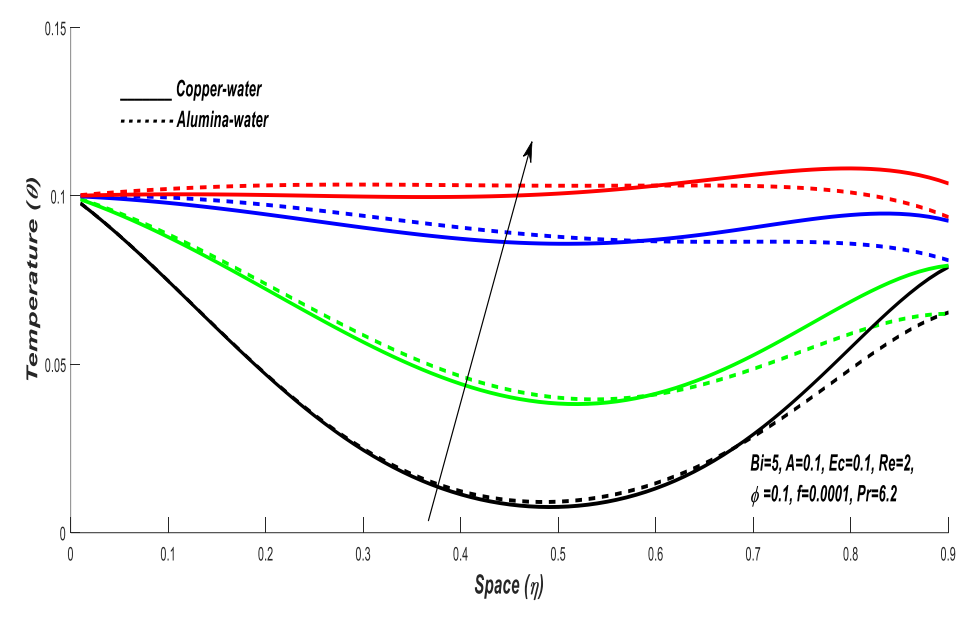


Fig. 8: Temperature profile of Nanofluids with increasing space

In Figure 9, it is observed that an increase in the Eckert number leads to a rise in the temperature profile. This temperature increase can be attributed to viscous dissipation at the flow boundaries and the characteristics of the channel flow. Specifically, the results show that at the lower plate of the channel, the temperature remains nearly unchanged despite variations in the Eckert number, whereas at the upper plate, a significant increase in temperature is observed in response to the rising Eckert number. This behavior may be explained by the interaction between the flow's kinetic energy and the channel's boundary layer.

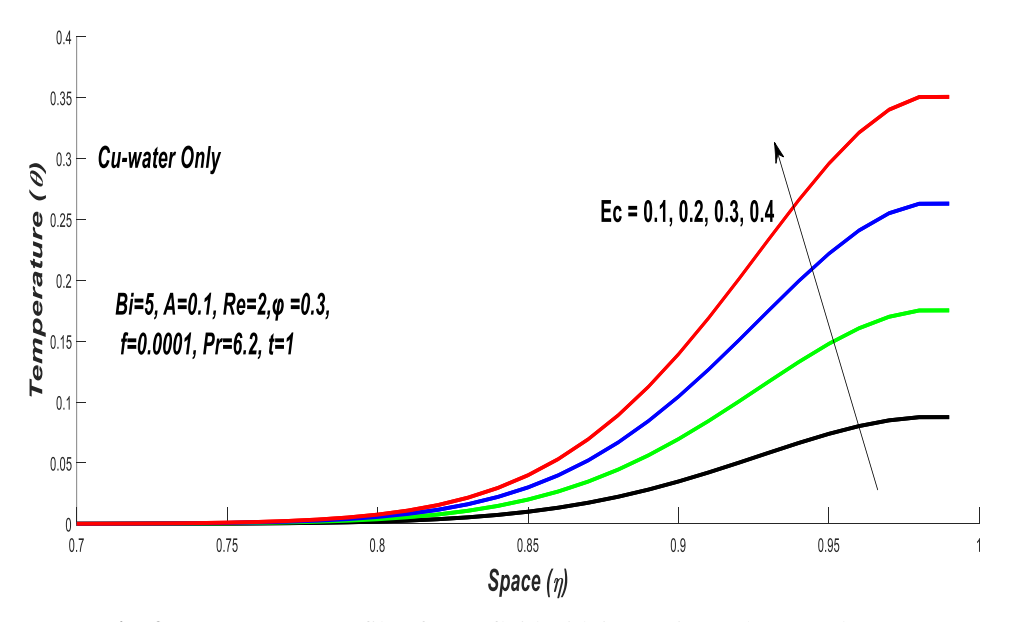


Fig. 9: Temperature Profile of Nanofluid with increasing Eckert number (Ec)

Figure 10 illustrates that an increase in the Biot number leads to a rise in the temperature profile. This increase can be attributed to viscous dissipation at the flow boundaries and the characteristics of the channel flow. Specifically, the results

show that at the lower plate of the channel, the temperature remains nearly unchanged despite variations in the Biot number, whereas at the upper plate, a significant temperature increase occurs in response to the rising Biot number. This behavior can be explained by the interaction between the flow's kinetic energy and the channel's boundary layer. Additionally, a higher Biot number corresponds to enhanced convective heat transfer to the surrounding environment, resulting in greater cooling at the wall and influencing the overall temperature distribution of the bulk nanofluid.

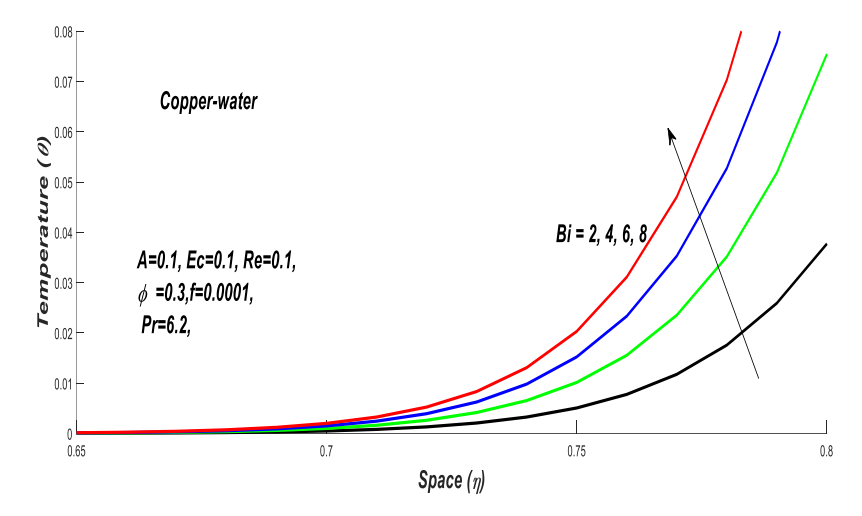


Fig. 10: Temperature Profile of Nanofluid with increasing Biot number (Bi)

From Figure 11, it is observed that the temperature profile at the lower plate increases with an increase in the nanoparticle volume fraction (Φ) . This rise in temperature can be attributed to the fact that the lower plate is stationary, resulting in a high frictional force that resists the motion of the copper-water nanoparticles and generates heat. Conversely, near the upper plate, the temperature remains largely unchanged even when the nanoparticle volume fraction (Φ) varies, due to the reduced frictional effects in that region.

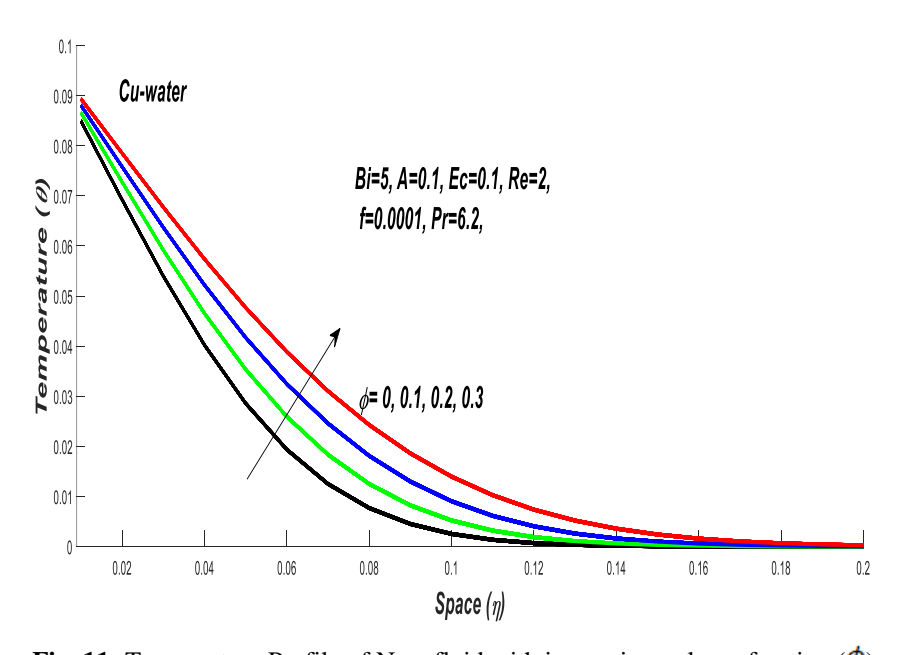


Fig. 11: Temperature Profile of Nanofluid with increasing volume fraction (ϕ)

Figure 12 shows a similar trend, where the temperature increases with an increase in the slip parameter. This behavior can be attributed to the slippage at the channel walls. Specifically, at the lower plate, the temperature remains nearly constant despite variations in the slip parameter, whereas at the upper plate, a significant increase in temperature is observed in response to the rising slip parameter. This phenomenon may be explained by the interaction between the flow's kinetic energy and the boundary layer of the channel.



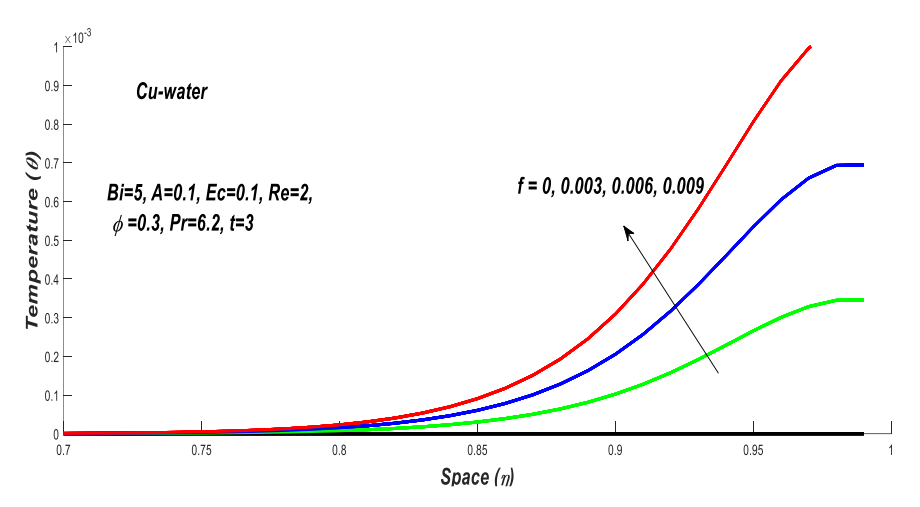


Fig. 12: Nanofluid temperature Profile with increasing slip parameter(f)

4 Conclusions

A numerical investigation of the effects of wall permeability on unsteady generalized Couette flow of nanofluids using copper and alumina as nanoparticles with convective heating is presented. The problem was solved numerically using a semi-discretization method combined with the Runge-Kutta integration technique. The key findings from the study are summarized as follows:

- An increase in nanoparticle volume fraction and Reynolds number leads to a rise in velocity when the pressure gradient, MHD effects, and nanofluid fraction are held constant.
- Alumina-water nanofluid exhibits a faster increase in the velocity profile compared to copper-water nanofluid.
- An increase in the Eckert number results in a decrease in the temperature profile.
- Copper-water nanofluid shows a faster rise in temperature compared to alumina-water nanofluid.

References

- [1] S. Yasutomi, S. Bair and W. Winer, An Application of a Free Volume Model to Lubricant Rheology: Independence of Viscosity on Temperature and Pressure. Journal of Tribology **106(2)**, 291-30, 1984.
- [2] S. Das, R. N. Jana, and A. J. Chamkha, Entropy generation due to unsteady hydromagnetic Couette flow and heat transfer with asymmetric convective cooling in a rotating system, J. Math. Model. **3** (2) 107-128, 2015.
- [3] S. U. S. Choi and J. A. Eastman, Enhancing thermal conductivity of fluids with nanoparticles, Proc. Journal of ASME Int. Mech. Eng. Congress and Exposition, San Franciscos, 99–105, 1995.
- [4] W. N. Mutuku and O. D. Makinde, Combined Effect of Buoyancy Force and Navier Slip on MHD Flow of a Nanofluid over a Convectively Heated Vertical Porous Plate. Theo. Nanoscience. **11(3)**, 667-675, 2013.
- [5] X. Wang and A. S. Mujumdar, Heat transfer characteristics of nanofluids: a review. International Journal of Thermal Sciences, **46(1)**, 1-19, 2007.
- [6] O. Kigodi, M. H. Mkwizu, A. X. Matofali, M. A. Selemani, N. Ainea, S. Khamis, and G. K. Karugila, Numerical investigation of entropy generation in unsteady MHD generalized Couette flow with convective cooling, Communication in Mathematical Modeling and Applications, 4(3), 95-111, 2019.
- [7] S. Choi, Z. Zhang, W. Yu, F. Lockwood and E. Grulke, Anomalous thermal conductivity enhancement in nanotube suspensions. Applied Physics Letters**79(14)**, 2252-2254, 2001.
- [8] M. H. Mkwizu, O. D. Makinde, and Y. Nkansah-Gyekye, Effects of Navier slip and wall permeability on entropy generation in unsteady generalized Couette flow of nanofluids with convective cooling, Journal of Applied Mathematics and Physics, 77 (4), 1454-2358, 2015.
- [9] I.Khan and A.M. Alqahtani, MHD model of nanofluids in a permeable channel with porosity. Symmetry, 11(3),



- [10] A.Noghrehabadi, M. R. Saffarian, and R. Pourrajab, Entropy analysis for nanofluid flow over a stretching sheet in the presence of heat generation/absorption and partial slip. Journal of Mechanical Science and Technology, **27(3)**, 927–937,2013.
- [11] S. Khamis, O. D. Makinde and Y. Nkansah-Gyekye, Modelling the Effects of Variable Viscosity in Unsteady Flow of Nanofluids in a Pipe with Permeable Wall and Convective Cooling. Applied and Computational Mathematics 3(3), 75-84, 2014.
- [12] O. D. Makinde and D. Theuri, Thermodynamic analysis of variable viscosity MHD unsteady generalized Couette flow with permeable walls, Applied and Computational Mathematics, **3**(1), 1-8, 2014.
- [13] H. F. Oztop and E. Abu-Nada, Numerical study of natural convection in partially heated rectangular enclosures filled with nanofluids, Int. Journal of Heat Fluid Flow, **29** (**5**), 1326–1336, 2008.